Radiological Physics and Technology (2019) 12:161–171
https://doi.org/10.1007/s12194-019-00507-9

Investigation of anisotropic fishing line-based phantom as tool in quality control of diffusion tensor imaging

Edna Marina de Souza[1,2,3,4] · **Eduardo Tavares Costa**[1,2] · **Gabriela Castellano**[3,4]

Received: 25 October 2018 / Revised: 6 March 2019 / Accepted: 7 March 2019 / Published online: 16 March 2019
© Japanese Society of Radiological Technology and Japan Society of Medical Physics 2019

Abstract

This work proposes a low-cost, fishing line-based phantom for quality control of diffusion tensor imaging (DTI). The device was applied to investigate the relationship between DTI indexes (DTIi) and imaging acquisition parameters. A Dyneema® fishing line phantom was built with fiber bundles of different thicknesses. DTI acquisitions were performed in a 3T magnetic resonance imaging scanner using an 8-channel and a 32-channel head coil. For each coil, the following acquisition parameters were changed, one at a time: diffusion sensitivity factor (*b* value), echo time, sensitivity encoding, voxel size, number of signal averages, and number of diffusion gradient directions (NDGD). DTIi including fractional anisotropy, relative anisotropy (RA), linear anisotropy (CL), and planar anisotropy (CP) were calculated for each image; the data were analyzed using the coefficient of variation (CV) and distributions of DTIi values. The 32-channel head coil presented higher CV values for the DTIi RA, CL, and CP when voxel size was changed. Using the phantom, dependences between diffusion-related parameters (*b* value and NDGD) and DTIi were also observed; the majority of these were for the smaller thickness fiber bundles. The device proved to be useful for the verification of the DTI performance over time.

Keywords MRI · DTI · Phantom · Quality control

1 Introduction

Diffusion tensor imaging (DTI) combines magnetic resonance imaging (MRI) techniques with diffusion measurements [1]. It is applied to the study of body structures under healthy and pathological conditions [2, 3]. Currently, it is known that DTI indexes (DTIi) are sensitive to factors related to image acquisition, such as magnetic field inhomogeneity, susceptibility effects, and eddy currents. These factors can present more detrimental effects on diffusion data than on T1 or T2 images [4]. In recent years, researchers have suggested different types of phantoms for quality control (QC) of diffusion imaging techniques. Some groups have used phantoms for isotropic diffusion, usually consisting of spheres or cylinders filled with liquids or gels [5, 6]. Others have used fiber phantoms made of microcapillary arrays permeated by liquids to simulate axonal tracts or cardiac muscles [7–9]. Some researchers have used biological phantoms, such as green asparagus inside a water container or animal tissues [10, 11]. Among the variety of materials for building DTI phantoms, Dyneema®, a fiber composed of ultrahigh-molecular weight polyethylene, has been suitable to simulate anisotropic structures [12–14]. These fibers possess a lower surface relaxivity [15–17], which results in overall longer relaxation times; this enables diffusion measurements to be collected with a higher signal-to-noise ratio (SNR) or longer echo time (TE). This is especially important in the case of strong diffusion weightings and time-dependent studies.

✉ Edna Marina de Souza
ednamarina.souza@gmail.com

Eduardo Tavares Costa
educosta@ceb.unicamp.br

Gabriela Castellano
gabriela@ifi.unicamp.br

[1] Biomedical Engineering Center, University of Campinas (UNICAMP), 163 Alexander Fleming St, Cidade Universitária, Campinas, SP 13083 881, Brazil

[2] Biomedical Engineering Department, School of Electrical and Computer Engineering, University of Campinas (UNICAMP), Campinas, Brazil

[3] Neurophysics Group, Gleb Wataghin Physics Institute, University of Campinas (UNICAMP), 777 Sergio Buarque de Holanda St, University City, Campinas, SP 13083 859, Brazil

[4] Brazilian Institute of Neuroscience and Neurotechnology (BRAINN), Campinas, Brazil

Until now, only Dyneema® raw fibers have been used to build anisotropic diffusion phantoms; thus, the present work proposes a low-cost Dyneema® fishing line-based phantom for the QC of DTI. The phantom was applied to study the influence of the acquisition parameters such as diffusion sensitivity factor (*b* value), TE, number of signal averages (NSA), sensitivity encoding (SENSE), voxel size, and number of diffusion gradient directions (NDGD) on the following DTIi: fractional anisotropy (FA), relative anisotropy (RA), linear anisotropy (CL), planar anisotropy (CP), mean diffusivity (MD), volume ratio (VR), and spherical anisotropy (CS) [18]. The influence of the fiber bundle thickness was also considered.

2 Materials and methods

2.1 Phantom construction

The phantom consisted of a cylindrical acrylic container with a height of 200 mm, and external and internal diameters of 180 mm and 170 mm, respectively, where a diffusion evaluation module (DEM) was inserted, consisting of a rectangular hollow section of 180×120 mm^2 and a wall thickness of 10 mm. The DEM had 18 circular holes of 10 mm in diameter and 18 circular holes of 20 mm in diameter regularly distributed over its sides, where the fiber bundles were positioned (Fig. 1a). The holes could also be useful to estimate geometric distortion effects. The DEM geometry and dimensions held the module fixed to the container to reduce the effects of unwanted vibrations due to the application of magnetic field gradients during the measurements.

Three fiber bundles with a length of 190 mm, composed of Dyneema® fishing lines, and identified as B1, B2, and B3, were positioned at three of the 20-mm-diameter holes (Fig. 1b). These bundles, respectively, possessed 200 fibers (fishing lines) of 0.25 mm diameter, 150 fibers of 0.35 mm diameter, and 130 fibers of 0.40 mm diameter (specifications provided by manufacturer). The compression and fixation of the bundles were achieved using nylon cable ties, causing the three bundles to have approximately the same average thickness: (17.5 ± 1.20) mm for bundle B1, (16.81 ± 0.95) mm for bundle B2, and (16.45 ± 2.01) mm for bundle B3, measured using a digital caliper. The container was filled with distilled water, with a diffusivity of 2.2×10^{-3} mm^2/s at room temperature [14].

The phantom was designed under the following constraints: simple to manufacture, constructed from readily available material, simple to use, robust, and providing a fixed geometry. Its dimensions were defined to fit inside MRI head coils. Dyneema® fishing lines were selected as they are MRI compatible [12], anisotropic, and less susceptible to the effects of gradient variations than microfabricated structures and other types of fibers. Furthermore, they have greater availability and lower cost than other types of materials. Intentionally, the bundles were not completely straight, because in the majority of biological tissues the tracts are disposed according to anatomical contours.

2.2 Imaging acquisition and processing

All images were acquired on the axial plane, in an Achieva® 3T MRI scanner (Philips Medical Systems, Cleveland, Ohio, United States) located at the Clinics Hospital of the University of Campinas (UNICAMP), using an 8-channel and a 32-channel head coil. The phantom was placed in the scanner's room 72 h before acquisitions to avoid temperature variation effects. For all acquisitions, the position of the phantom was identical. Its center was aligned by a laser with the center of each coil and the DTI measurements were acquired changing the following parameters, one at a time, using the clinical acquisition protocol as a standard:

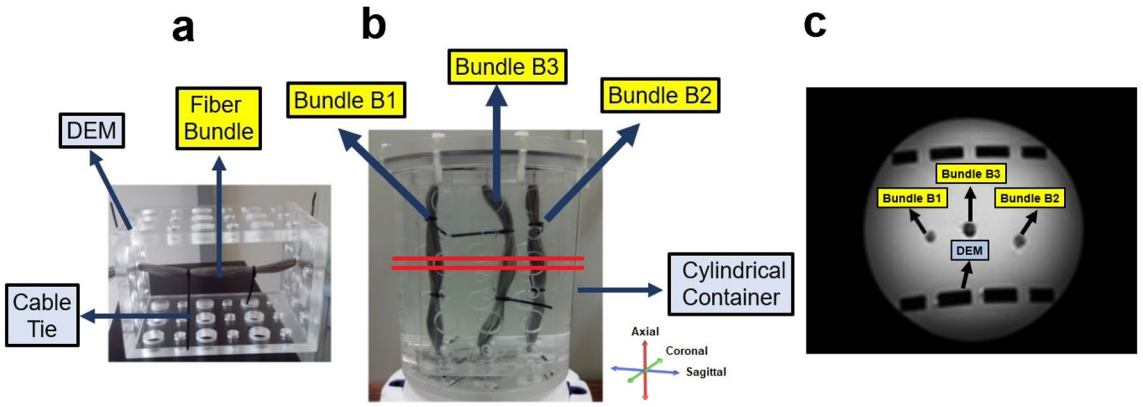

Fig. 1 Pictures of the DTI phantom. **a** DEM with one fiber bundle positioned. **b** Phantom mounted and filled with distilled water. The red lines highlight the orientation of the axial plane. **c** DWI acquired in the axial plane using the 32-channel head coil and $b = 2500$s/mm^2

Table 1 DTI acquisition standard parameters for both coils and the variations tested in this study

Acquisition parameter	Standard Protocol	Variations
b (s/mm^2)	1000	500/800/1000/1200/1500/2000/2500
TE (ms)	85	70/80/85/90/100
NSA	1	1/2/4/6
SENSE	2.5	2/2.5/2.8/3/3.5/3.8
Voxel size (mm^3)	2	1/1.5/2/2.5/3
NDGD	32	6/15/32

b, TE, NSA, SENSE, voxel size, and NDGD. The variations of parameters were identical for both coils, as presented in Table 1.

During the 7 months of data collection, two DTI using the standard protocol were obtained at the beginning of each experiment session. The phantom reproducibility was assessed from the mean and the CV values of the calculated MD and FA, considering all fiber bundles and both coils.

Before DTIi estimation, all images acquired with identical parameters, i.e., the non-diffusion-weighted image (T2) and all diffusion-weighted images (DWI), were co-registered using mutual information maximization-based algorithms implemented in the MRI scanner. This step reduces the effects of vibration and motion during patients' scans. However, for this phantom study, there were no visual differences between the images before and after co-registration. Nevertheless, non-visible differences due to vibration, which could affect DTIi, could be present; therefore, the co-registration step was maintained.

Afterwards, the DTI measurements were submitted to the QC routines of the ExploreDTI software [19, 20], which employs calculations based on a residual model and creates image outlier maps to detect distortions that could lead to bias in DTIi. For images without significant outliers, ExploreDTI was also used to manually draw seed regions of interest (ROIs) in the coronal plane, one for each fiber bundle and each DTI measurement acquired (Fig. 2). From these ROIs, the eigenvalues (λ_1, λ_2, and λ_3) were calculated and the tract reconstructions were generated.

2.3 DTIi calculation and data analysis

The calculation of the DTIi was performed from λ values, using Matlab® (version R2014b, Matlab Inc., Natick, MA, USA) routines. The data analysis (DTIi distributions analysis and CV calculation) was performed using SPSS (version 22; SPSS Inc., Chicago, IL, USA); for each bundle, each coil, and each acquisition parameter changed.

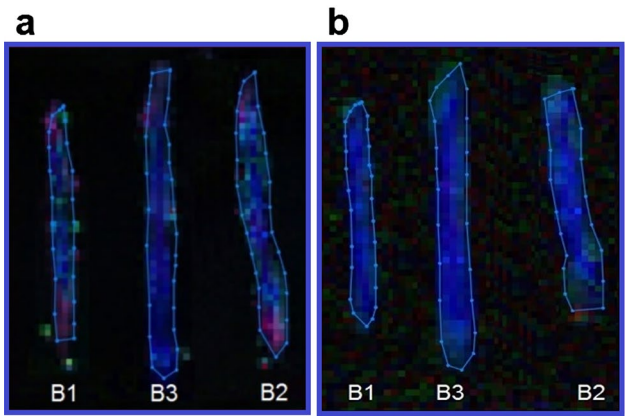

Fig. 2 Examples of seed ROIs on the coronal plane of DTI for the determination of tensor eigenvalues for each fiber bundle. **a** b value = 500 s/mm^2. **b** b value = 2500 s/mm^2 (eight-channel head coil). The color coding is based on water diffusion orientation (red: right–left, blue: dorsal–ventral, and green: anterior, posterior)

3 Results

3.1 Phantom stability evaluation

Considering all acquisitions, for the eight-channel head coil, the mean of MD values for bundles B1, B2, and B3 was $(1.43 \pm 0.01) \times 10^{-3}$ mm^2/s, $(1.42 \pm 0.03) \times 10^{-3}$ mm^2/s, and $(1.36 \pm 0.04) \times 10^{-3}$ mm^2/s, respectively, and the FA values were (0.34 ± 0.003), (0.39 ± 0.005), and (0.43 ± 0.002), respectively. For the 32-channel head coil, the MD values were $(1.46 \pm 0.03) \times 10^{-3}$ mm^2/s, $(1.49 \pm 0.06) \times 10^{-3}$ mm^2/s, and $(1.38 \pm 0.04) \times 10^{-3}$ mm^2/s, respectively, and the FA values were (0.31 ± 0.002), (0.32 ± 0.001), and (0.40 ± 0.001), respectively.

Figure 3 presents the CV values of MD and FA obtained in this step of the study. For both coils and all bundles, these values were lower than 5%, indicating that the MD and FA values remained stable over time under identical image acquisition conditions, reflecting the phantom reproducibility.

3.2 DTIi distribution analysis

Figure 4 presents boxplots for MD and FA for the 8-channel and 32-channel head coils. For MD and the eight-channel head coil, the highest variations of values, for the same fiber bundle (B3), are observed when the voxel size is changed, followed by b and NDGD. An analogous behavior is observed for the FA values. For the 32-channel head coil, identical acquisition parameters produce the highest variations of MD, which demonstrates a broader range of values when b is changed.

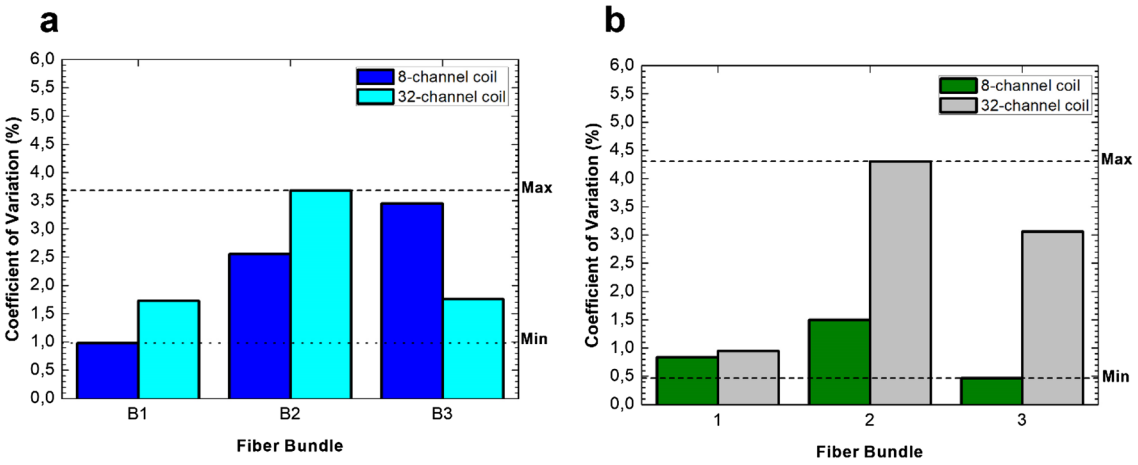

Fig. 3 CV values of **a** MD and **b** FA for the evaluation of phantom reproducibility

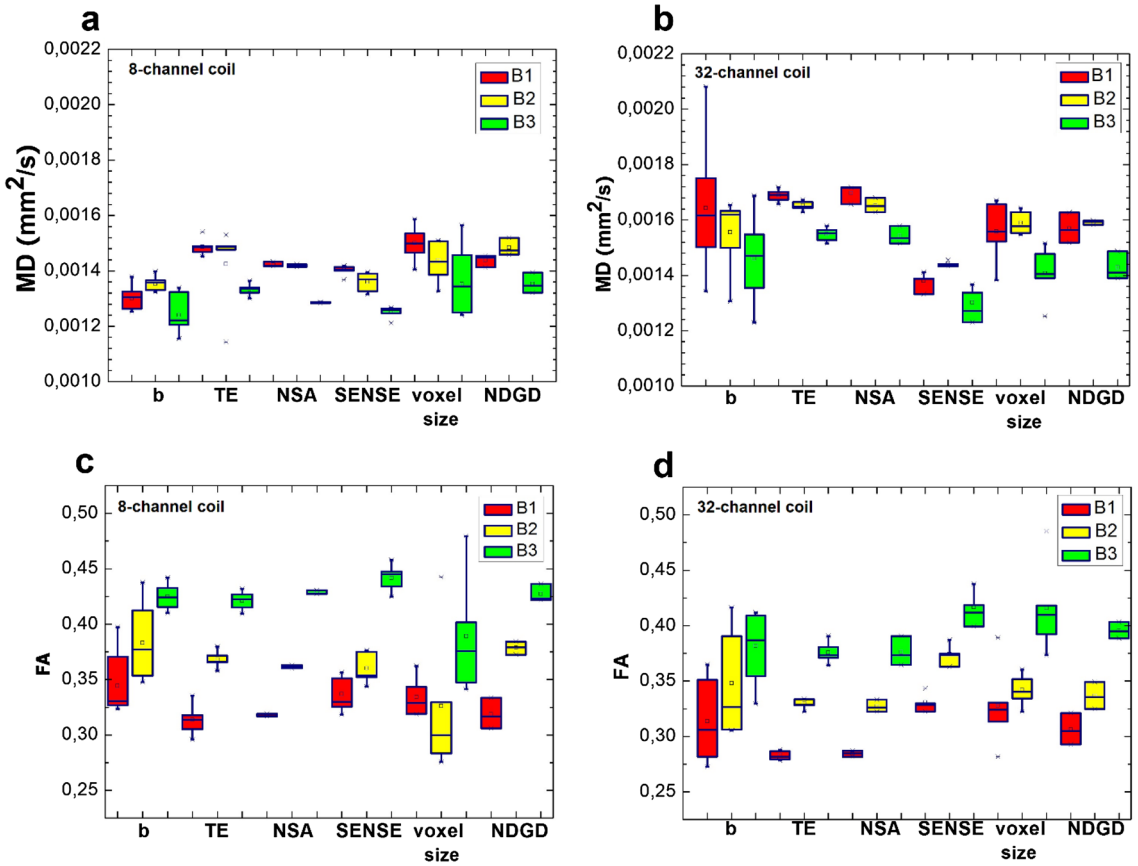

Fig. 4 Boxplots of MD and FA for the 8-channel (**a, c**), and 32-channel (**b, d**) head coils, considering fiber bundles B1 (red), B2 (yellow), and B3 (green)

Figure 5 presents boxplots for RA and VR for the 8-channel and 32-channel head coils. The SENSE and NSA modifications produce higher variations of the RA and VR values for the 8-channel and 32-channel head coil, respectively, followed by b, which influences all DTIi values.

Figure 6 presents boxplots for CS, CL, and CP for the 8-channel and 32-channel head coils. The geometric indices,

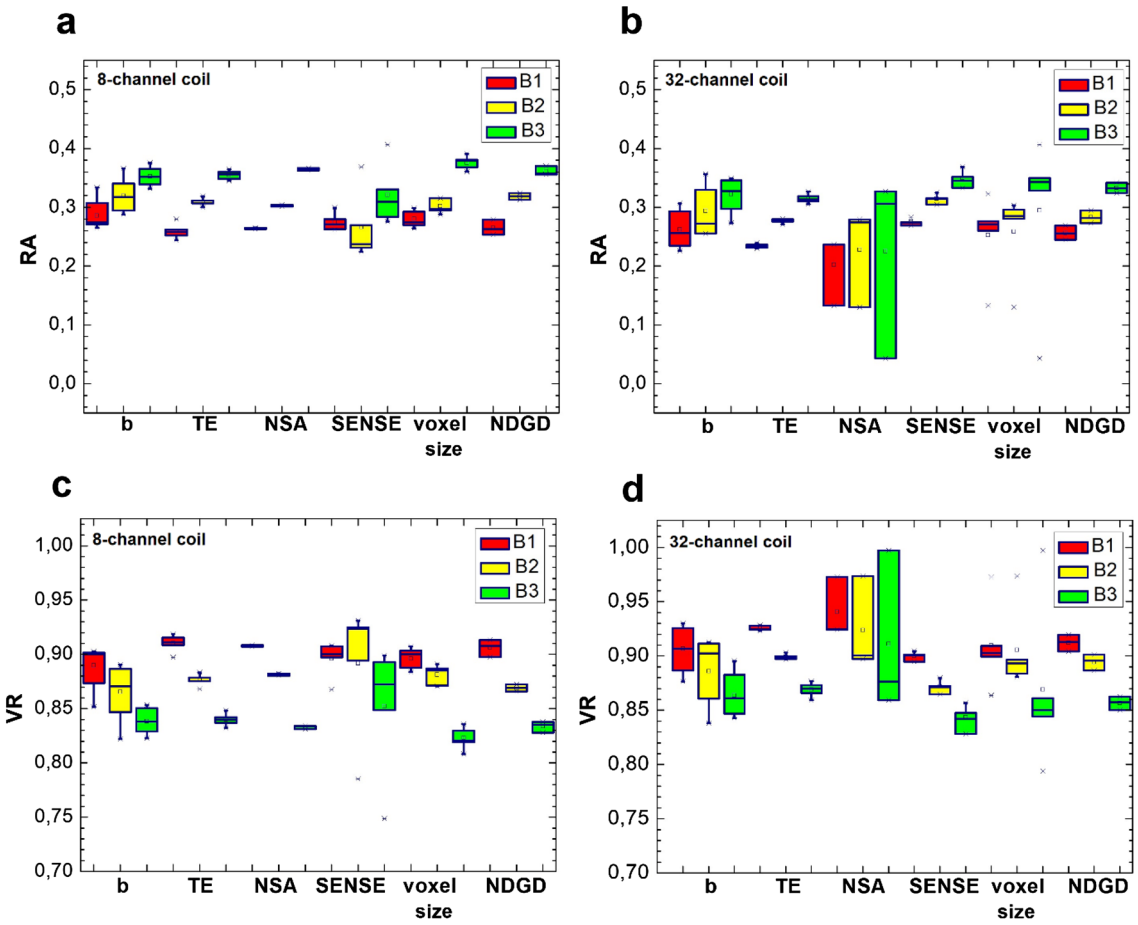

Fig. 5 Boxplots of RA and VR for the 8-channel (**a, c**) and 32-channel (**b, d**) head coils, considering fiber bundles B1 (red), B2 (yellow), and B3 (green)

CS and CP, demonstrate the largest range of values when NSA and SENSE are changed, followed by *b*. For the 8-channel head coil, additional variations of CS and CP are observed when SENSE is modified, while for the 32-channel head coil, larger variations of CS, CL, and CP are obtained when NSA is modified. For the eight-channel head coil, a larger range of CL values is obtained when b or NDGD are varied.

3.3 CV analysis

Figure 7 presents the CV values of DTIi for bundles B1, B2, and B3, with varied acquisition parameters for each coil used. The highest CV values are primarily observed for the geometric DTIi CL and CP, for all bundles and coils used. Among these values, the highest CV is observed for CP (75.26%) for the NSA changes, considering B2 and the eight-channel head coil (Fig. 7c). For B1 and the eight-channel head coil (Fig. 7a), the highest CV value is obtained for CP (66.74%), for the NSA changes. Considering still bundle B1, but with the 32-channel head coil (Fig. 7b), the highest CV values are observed for CL and CP, for the voxel size variation (56.12% and 55.24%, respectively). In this case, the modifications of b and SENSE also produce higher CV values of CP (45.95% and 40.61%, respectively).

For bundle B2 and the acquisitions with the 32-channel head coil (Fig. 7d), the highest CV value is obtained for CP when the voxel size is changed (59%). The bundle B3 and the eight-channel head coil acquisitions (Fig. 7e) result in higher CV values for CP when TE, NDGD, b, and SENSE are modified (24.95%, 23.23%, 20.68%, and 14.59%, respectively). Still for bundle B3, but with the 32-channel head coil (Fig. 7f), the voxel size variation and SENSE alterations result in higher CV values for CL, CP, and RA (72.78%, 53.22%, and 70.15%, respectively, for voxel size, and 67.75%, 37.75%, and 48.75%, respectively for SENSE).

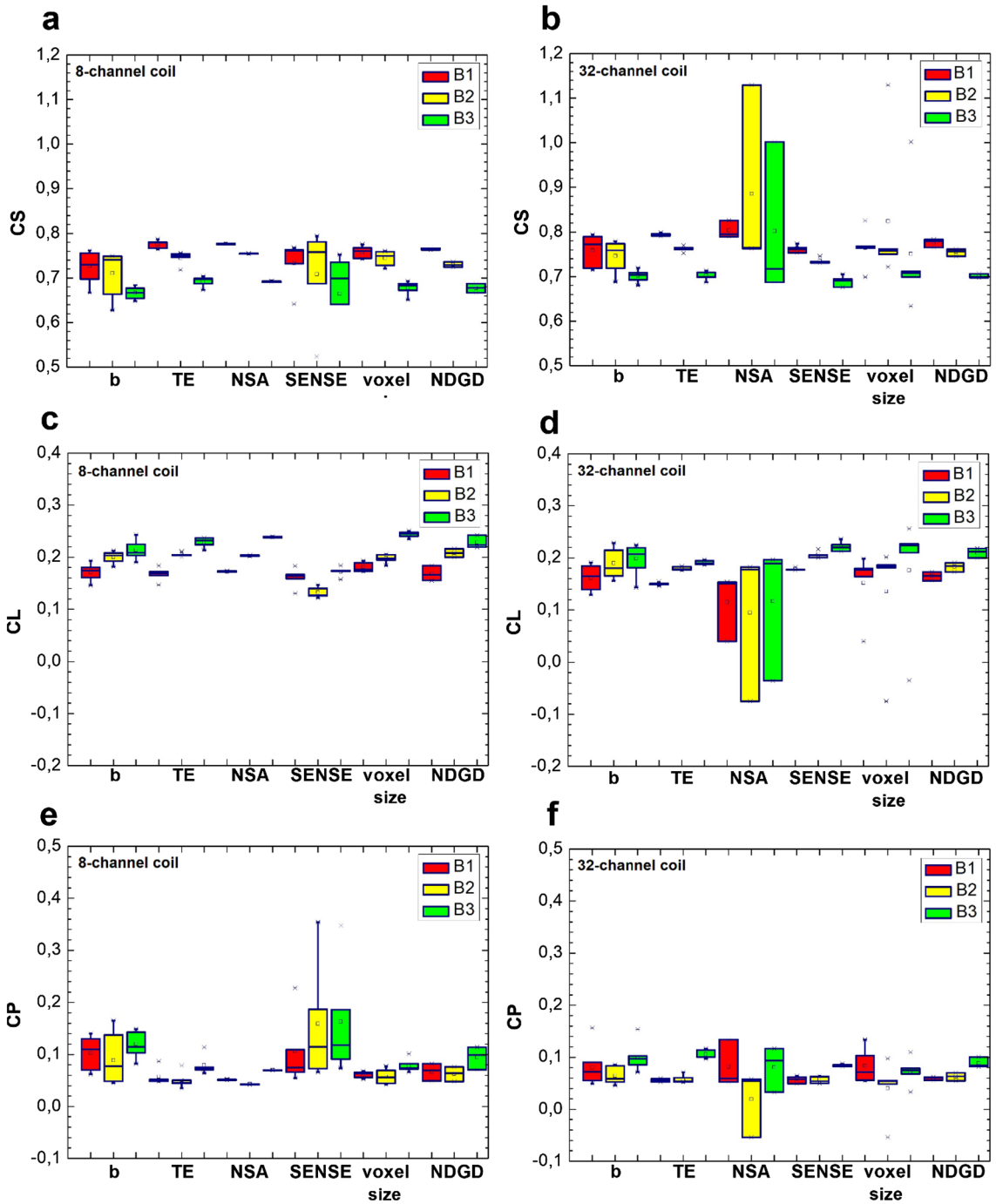

Fig. 6 Boxplots for CS, CL, and CP for the 8-channel (**a, c, e**) and 32-channel (**b, d, f**) head coils, considering fiber bundles B1 (red), B2 (yellow), and B3 (green)

3.4 Diffusion ellipsoids and tract reconstructions

Figures 8 and 9 show examples of how the DTI acquisition parameter variations can visually change the diffusion ellipsoids and reconstruction of tracts. Figure 8 presents examples of diffusion ellipsoids and tracts estimated from seed ROIs defined in the ExploreDTI software, for both coils and different values of NDGD. All fiber bundles are displayed in all images. However, for both coils, the lower thickness bundle, B1, is not properly visualized in all slices for NDGD = 6. For NDGD = 32, all bundles are well defined. For lower NDGD values, the 8-channel coil exhibits less background noise than the 32-channel coil.

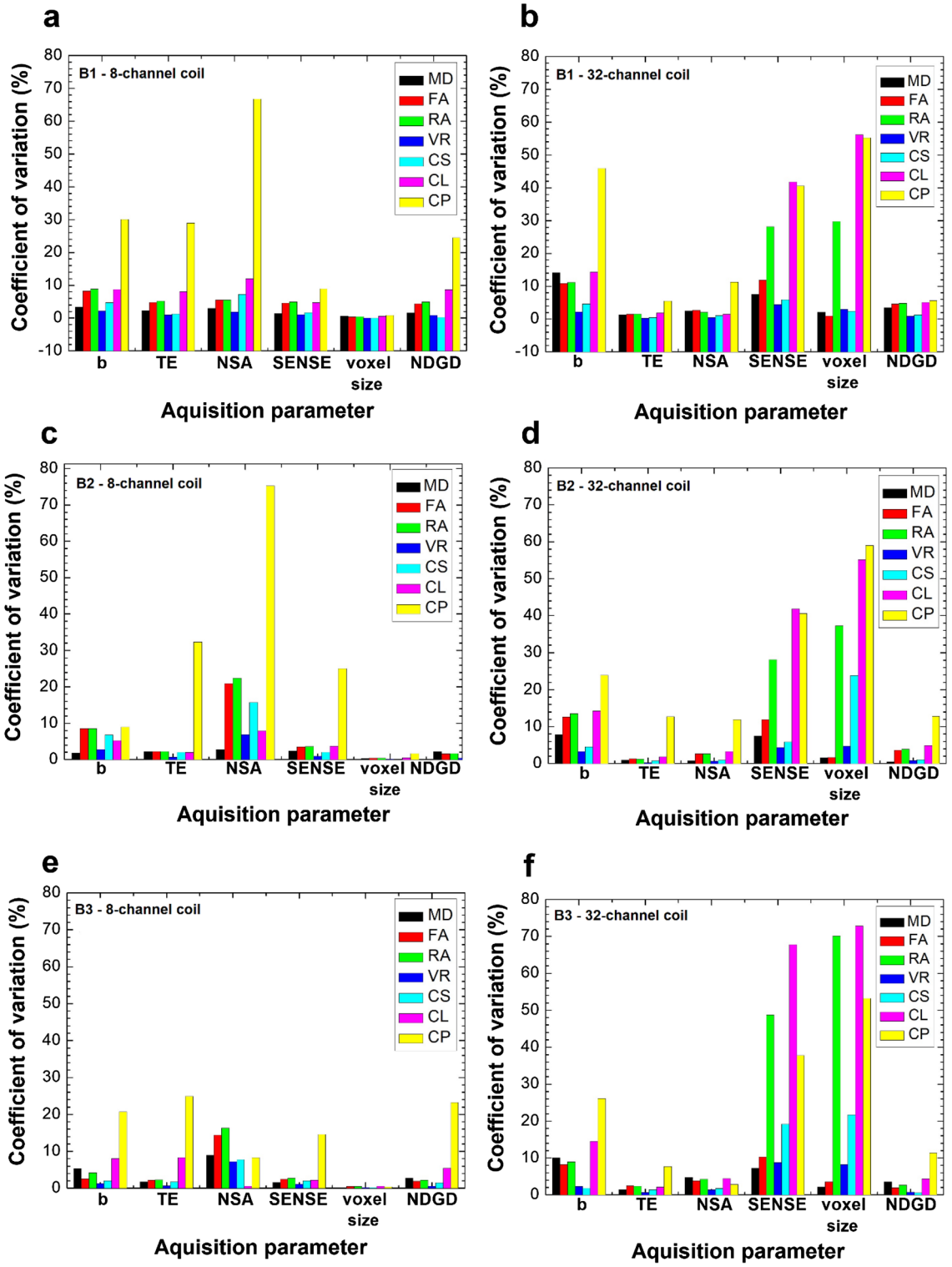

Fig. 7 CV values of the DTIi obtained from bundles B1, B2, and B3, for the 8-channel (**a, c, e**, respectively) and 32-channel (**b, d, f**, respectively) head coil

In Fig. 9, examples of tract reconstructions for acquisitions changing the *b* value are displayed. It can be observed that for b = 500 s/mm^2, bundles B1 and B2 are not displayed from the DTI data acquired with the 8-channel head coil (Fig. 9a). Furthermore, for this *b* value and coil, the bundles are thinner than for the 32-channel head coil. For b = 1500 s/

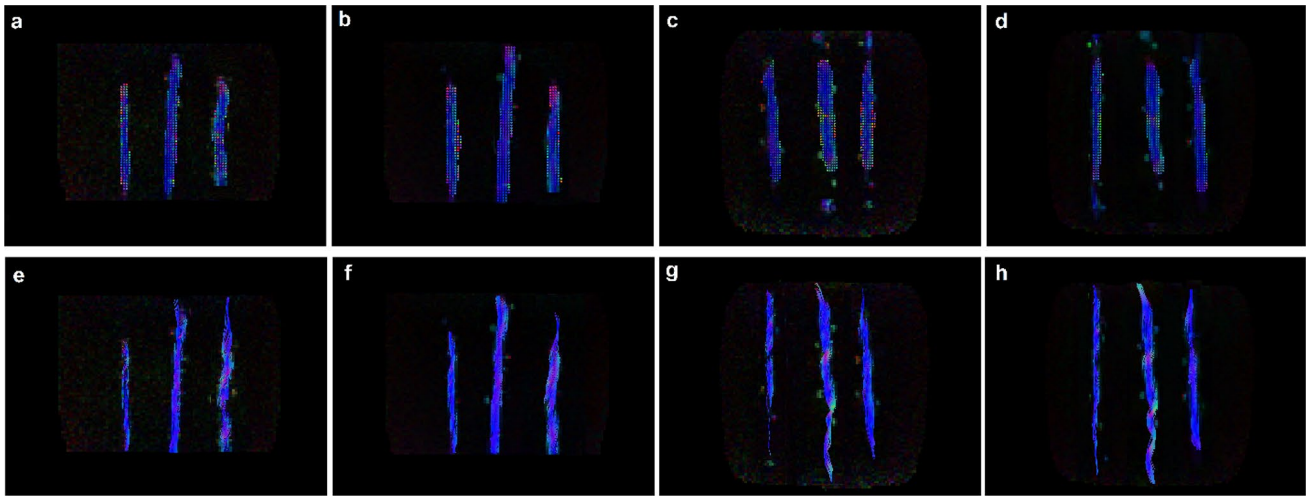

Fig. 8 Examples of diffusion ellipsoids (upper line) and tracts (lower line) calculated from seed ROIs defined in the ExploreDTI software. **a, e** 8-channel head coil, NDGD = 6. **b, f** 8-channel head coil, NDGD = 32. **c, g** 32-channel head coil, NDGD = 6. **d, h** 32-channel head coil, NDGD = 32. In each image, the bundles B1, B2, and B3 are displayed on the left, in the middle, and on the right, respectively. The color coding of tractography was applied, according to diffusion orientation (red: right–left, blue: dorsal–ventral, and green: anterior–posterior)

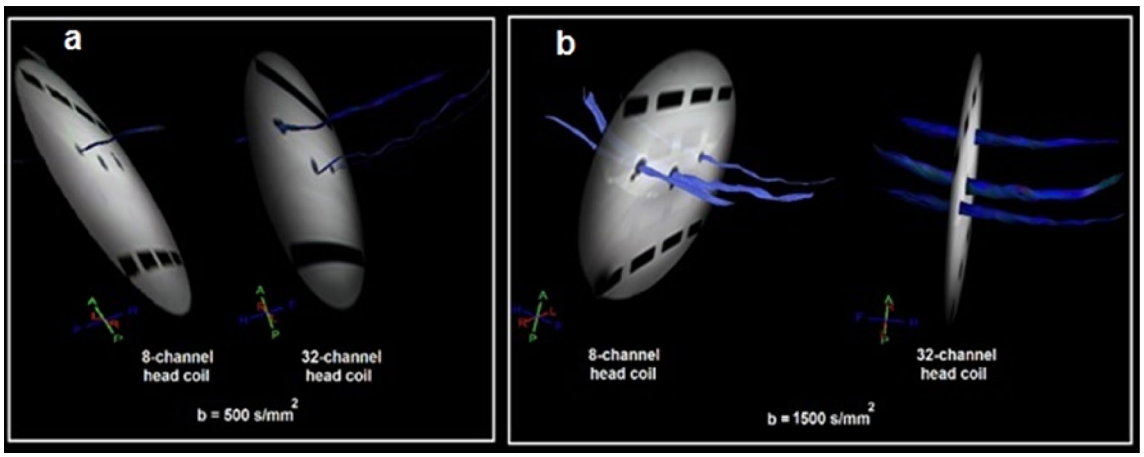

Fig. 9 Reconstructions of the tracts for acquisitions changing the *b* value, for the 8-channel and 32-channel head coils. *b* values used: **a** 500 s/mm^2, and **b** 1500s/mm^2

mm^2, all bundles could be visualized (Fig. 9b), from acquisitions using either the 8- or the 32-channel head coils. Similar results are obtained with NDGD = 6 and 32, respectively.

4 Discussion

In this work, we proposed and developed a Dyneema® fishing line-based fiber phantom for DTI QC and applied the device to verify the influence of the acquisition parameters on DTIi. The evaluation of MD and FA values of each fiber bundle from DTI acquired using the standard protocol, at the beginning of each session of acquisitions, demonstrates that the phantom is stable over time and can be applied as a tool for assessing the DTIi stability.

The primary advantages of Dyneema® fishing lines to build fiber phantoms are the higher impermeability (enabling the simulation of biological anisotropic diffusion) and the higher viscosity (which reduces the effects of convective motion) than other materials, such as polyamide fishing lines. Dyneema® fibers are easy to handle, rendering it possible to build bundles in multiple configurations (e.g., straight, twisted, compacted, or mixed arrangements), preserving the diffusion characteristics. Furthermore, these fibers are strong, biocompatible, and are used in vascular prostheses and suture in tendons and ligaments [21], structures

commonly evaluated by MRI. The proposed phantom also tends to be more stable because inside the fishing lines the fibers are already organized in a multifilament, favoring the confection of uniform bundles. Finally, the proposed phantom is a lower cost device than other phantoms composed of microfabricated structures, which present more DTIi variations due to the EPI effects, even for acquisitions using identical parameters [8]. The holes of the DEM can also be used for the evaluation of geometric distortion effects and the water-filled portion of the cylinder can be used to check the quality of isotropic diffusion data.

For the primary white matter tracts of the normal brain, the FA values range from 0.4 to 0.8 [2, 22]. According to previous studies [23, 24], the FA values of the phantom bundles determined here are near the range observed in brain tissues and in the range of cardiac muscle. However, the values determined here for MD were out of the range observed for human brain tissues [25]. This is probably because the fibers used in the phantom have a higher impermeability than axon tracts, therefore, affecting the MD. Nevertheless, the FA and MD values of the bundles can be improved by increasing the compression of the bundles and using a $CuSO_4$-based solution for MRI phantoms. However, the difference in values did not compromise the device performance.

As expected, we observed that the geometric DTIi was more sensitive to the variations of the DTI acquisition parameters (especially voxel size, NSA, and SENSE) than the other indices. The highest CV values were observed for the 32-channel head coil and the DTIi RA, CL, and CP, when NSA was changed for bundle B3. The NSA directly affects the SNR, which can influence the DTIi [26]. These facts can explain the higher CV values for CL and CP (which are geometric DTIi), and even for RA, in contrast to results demonstrated in [26]. However, it remains unclear why the 32-channel coil was affected more than the 8-channel coil. A hypothesis is that for the 32-channel coil, the larger distance between the DEM and the coil elements could produce image distortions in the phase-encoding direction.

The analysis of DTIi distributions demonstrated relations between the parameters of the diffusion weight (b and NDGD) and the DTIi, as previously described in [7]. For fiber bundles having a lower thickness, this effect was more significant. Regarding the TE, the DWI are T2 weighted as the TE should be long enough to be compatible with the duration of diffusion gradients [27]. Therefore, DTIi, such as MD and FA, are expected to vary when the TE is changed [28]. However, an influence of the TE on DTIi was observed primarily for the 32-channel head coil, and only for bundles B2 and B3, which were composed of thicker fibers. This suggests that the contrast in those bundles was affected more by TE changes than in bundle B1. Moreover, the fact that the 32-channel head-coil can improve the SNR could also have contributed to this difference.

Indeed, a relation between the SENSE factor and DTIi was observed only for the 8-channel head coil, probably due to its lower SNR compared with the 32-channel coil, which reduced the effect of noise or geometric distortions due to SENSE. Furthermore, the higher number of channels also reduced the effects of the voxel size variation. This is probably due to the fact that for the 32-channel coil, there is a higher sensitivity to the volume of material near each coil channel, which collects more spatial information for data reconstruction.

The relation between the acquisition parameters and the DTIi is not clearly defined yet; neither are its causes. Although several studies exploring the relation between the acquisition parameters, and MD and FA are in the literature, there is no consensus between these studies as phantoms and acquisition set-ups are not identical. Several authors observed a relation between FA and voxel size and NDGD [29–31]; others, between FA and SENSE, b, or TE [31–33], or even no relationship between the DTIi and acquisition parameters [26, 34–36]. The majority of those studies used image acquisitions of healthy subjects, which are not the most suitable choice to explore scanner parameters and performance characteristics due to the inherent variability of human tissues and the fact that we do not know the exact body composition of the subjects. Depending on the body region or tissue, different relations between acquisition parameters and DTIi have been observed [37].

The phantom presented here was designed for usage in a clinical MRI scanner, fitting inside head coils. Nevertheless, it can be scaled for other coils or MRI scanner types. It has been tested using DTI, despite the existence of more advanced diffusion-weighted MRI techniques; factors that compromise DTIi also tend to affect more accurate techniques, such as high-angular diffusion imaging [38], diffusion spectral imaging [39], and Q-Ball [40]. Furthermore, DTI is still widely applied in developing countries, where the present QC routines have been implemented.

These results must also be considered in the case of multiscanner or multicentric studies. In the future, we intend to use the phantom for the QC of other scanners, other diffusion-weighted MRI techniques, as well as for adapting the device for different types of coils.

5 Conclusion

The results of this study suggest that the proposed phantom can be used as a reference for assessing the DTIi over time. Given that the acquisition parameter variations can change DTIi, it is important to change the acquisition protocols carefully, avoiding comparisons of data acquired with different set-ups, primarily in studies of low-diameter fiber tracts.

Acknowledgements The authors would like to thank the staff at the Biomedical Engineering Center, School of Electrical and Computer Engineering (UNICAMP) for building the phantom, and the 3T MRI scanner of Clinics Hospital (UNICAMP) staff for assistance with scanner access.

Author contributions Study conception and design: EMS, ETC, GC. Acquisition of data: EMS. Analysis and interpretation of data: EMS, GC. Drafting of manuscript: EMS, ETC, GC. Critical revision: ETC, GC. Approval of the final version: EMS, ETC, GC.

Funding This work was supported by São Paulo Research Foundation (FAPESP, Brazil, Grant—2013/07559-3) through BRAINN (Brazilian Institute of Neuroscience and Neurotechnology), and by the National Council for Scientific and Technological Development (CNPQ, Brazil, Grant—310860/2014-8).

Compliance with ethical standards

Conflict of interest The authors declare that they have no conflict of interest.

Ethical approval This article does not contain any studies with human participants or animals performed.

References

1. Basser PJ, Mattiello J, LeBihan D. Estimation of the effective self-diffusion tensor from the NMR spin echo. J Magn Reson B. 1994;103(3):247–54.
2. Yoshida S, Oishi K, Faria AV, Mori S. Diffusion tensor imaging of normal brain development. Pediatr Radiol. 2013;43(1):15–27.
3. Sternberg EJ, Lipton ML, Burns J. Utility of diffusion tensor imaging in evaluation of the peritumoral region in patients with primary and metastatic brain tumors. AJNR. 2014;35(3):439–44.
4. Le Bihan D, Poupon C, Amadon A, Lethimonnier F. Artifacts and pitfalls in diffusion MRI. J Magn Reson Imaging. 2006;24(3):478–88.
5. Hellerbach A, Schuster V, Jansen A, Sommer J. MRI phantoms—are there alternatives to agar? PLoS One. 2013;8(8):e70343.
6. Zhu T, Hu R, Qiu X, Taylor M, Tso Y, Yiannoutsos C, Navia B, Mori S, Ekholm S, Schifitto G, Zhong J. Quantification of accuracy and precision of multi-center DTI measurements: a diffusion phantom and human brain study. Neuroimage. 2011;56(3):1398–411.
7. Kim SJ, Choi CG, Kim JK, Yun SC, Jahng GH, Jeong HK, Kim EJ. Effects of MR parameter changes on the quantification of diffusion anisotropy and apparent diffusion coefficient in diffusion tensor imaging: evaluation using a diffusional anisotropic phantom. Korean J Radiol. 2015;16(2):297–303.
8. Ebrahimi B, Swanson SD, Chupp TE. A microfabricated phantom for quantitative MR perfusion measurements: validation of singular value decomposition deconvolution method. IEEE Trans Biomed Eng. 2010;57(11):2730–2736.
9. Teh I, Zhou FL, Hubbard Cristinacce PL, Parker GJ, Schneider JE. Biomimetic phantom for cardiac diffusion MRI. J Magn Reson Imaging. 2015;43:594–600
10. Latt J, Nilsson M, Rydhog A, Wirestam R, Stahlberg F, Brockstedt S. Effects of restricted diffusion in a biological phantom: a q-space diffusion MRI study of asparagus stems at a 3T clinical scanner. Magma. 2007;20(4):213–22.
11. Komlosh ME, Lizak MJ, Horkay F, Freidlin RZ, Basser PJ. Observation of microscopic diffusion anisotropy in the spinal cord using double-pulsed gradient spin echo MRI. Magn Reson Med. 2008;59(4):803–9.
12. Fieremans E. Simulation and experimental verification of the diffusion in an anisotropic fiber phantom. J Magn Reson. 2008;190(2):189–199.
13. Lorenz R, Kreher BW, Hennig J, Anisotropic phantoms for quantitative diffusion tensor imaging and fib. In: Proceedings of ISMRM 14th scientific meeting. Seattle, USA; 2006.
14. Farrher E, Kaffanke J, Celik AA, Stocker T, Grinberg F, Shah NJ. Novel multisection design of anisotropic diffusion phantoms. Magn Reson Imaging. 2012;30(4):518–26.
15. Kleinberg RL. Utility of NMR T2 distributions, connection with capillary pressure, clay effect, and determination of the surface relaxivity parameter rho 2. Magn Reson Imaging. 1996;14(7–8):761–7.
16. Slijkerman WF, Hofman JP. Determination of surface relaxivity from NMR diffusion measurements. Magn Reson Imaging. 1998;16(5–6):541–4.
17. Lorenz R, Kreher BW, Henning J. P.o.I.t.S.M.. Anisotropic Fiber Phantom for DTI validation on a clinical scanner, ISMRM 14th Scientific Meeting, Seattle, USA; 2006. p. 1226.
18. Pierpaoli C, Basser PJ. Toward a quantitative assessment of diffusion anisotropy. Magn Reson Med. 1996;36(6):893–906.
19. Tournier JD, Mori S, Leemans A. Diffusion tensor imaging and beyond. Magn Reson Med. 2011;65(6):1532–56.
20. Leemans A, Jeurissen B, Sijbers J, Jones DK. ExploreDTI: a graphical toolbox for processing, analyzing, and visualizing diffusion MR data. In: 17th annual meeting of intl soc mag reson med, Hawaii, USA; 2009. p. 3537
21. Basir A, de Groot P, Grundeman PF, Tersteeg C, Maas C, Barendrecht A, van Herwaarden J, Kluin J, Moll F, Pasterkamp G, Roest M. In Vitro hemocompatibility testing of dyneema purity fibers in blood contact. Innovations (Phila). 2015;10(3):195–201.
22. Bennett IJ, Madden DJ, Vaidya CJ, Howard DV, Howard JH. Age-related differences in multiple measures of white matter integrity: a diffusion tensor imaging study of healthy aging. Hum Brain Mapp. 2010;31(3):378–90.
23. Poveda F, Gil D, Marti E, Andaluz A, Ballester M, Carreras F. Helical structure of the cardiac ventricular anatomy assessed by diffusion tensor magnetic resonance imaging with multiresolution tractography. Rev Esp Cardiol (Engl Ed). 2013;66(10):782–90.
24. Qin X, Wang S, Shen M, Zhang X, Wagner MB, Fei B. Mapping cardiac fiber orientations from high-resolution DTI to high-frequency 3D ultrasound. Proc SPIE. 2014;9036:90361O.
25. Helenius J, Soinne L, Perkio J, Salonen O, Kangasmaki A, Kaste M, Carano RA, Aronen HJ, Tatlisumak T. Diffusion-weighted MR imaging in normal human brains in various age groups. AJNR Am J Neuroradiol. 2002;23(2):194–9.
26. Widjaja E, Mahmoodabadi SZ, Rea D, Moineddin R, Vidarsson L, Nilsson D. Effects of gradient encoding and number of signal averages on fractional anisotropy and fiber density index in vivo at 1.5 T. Acta Radiol. 2009;50(1):106–13.
27. Bammer R. Basic principles of diffusion-weighted imaging. Eur J Radiol. 2003;45(3):169–84.
28. Fushimi Y, Miki Y, Okada T, Yamamoto A, Mori N, Hanakawa T, Urayama S, Aso T, Fukuyama H, Kikuta K, Togashi K. Fractional anisotropy and mean diffusivity: comparison between 3.0-T and 1.5-T diffusion tensor imaging with parallel imaging using histogram and region of interest analysis. NMR Biomed. 2007;20(8):743–8.
29. Santarelli X, Garbin G, Ukmar M, Longo R. Dependence of the fractional anisotropy in cervical spine from the number of diffusion gradients, repeated acquisition and voxel size. Magn Reson Imaging. 2010;28(1):70–6.

30. Giannelli M, Cosottini M, Michelassi MC, Lazzarotti G, Belmonte G, Bartolozzi C, Lazzeri M. Dependence of brain DTI maps of fractional anisotropy and mean diffusivity on the number of diffusion weighting directions. J Appl Clin Med Phys. 2009;11(1):2927.
31. Qin W, Yu CS, Zhang F, Du XY, Jiang H, Yan YX, Li KC. Effects of echo time on diffusion quantification of brain white matter at 1.5 T and 3.0 T. Magn Reson Med. 2009;61(4):755–60.
32. Alexander AL, Lee JE, Wu YC, Field AS. Comparison of diffusion tensor imaging measurements at 3.0 T versus 1.5 T with and without parallel imaging. Neuroimaging Clin N Am. 2006;16(2):299–309, xi.
33. Jones DK, Basser PJ. "Squashing peanuts and smashing pumpkins": how noise distorts diffusion-weighted MR data. Magn Reson Med. 2004;52(5):979–93.
34. Huisman TA, Loenneker T, Barta G, Bellemann ME, Hennig J, Fischer JE. K.A. Il'yasov, Quantitative diffusion tensor MR imaging of the brain: field strength related variance of apparent diffusion coefficient (ADC) and fractional anisotropy (FA) scalars. Eur Radiol. 2006;16(8):1651–8.
35. Melhem ER, Itoh R, Jones L, Barker PB. Diffusion tensor MR imaging of the brain: effect of diffusion weighting on trace and anisotropy measurements. AJNR. 2000;21(10):1813–20.
36. Klodowski K, Krzyzak AT. Innovative anisotropic phantoms for calibration of diffusion tensor imaging sequences. Magn Reson Imaging. 2016;34(4):404–9.
37. Vollmar C, O'Muircheartaigh J, Barker GJ, Symms MR, Thompson P, Kumari V, Duncan JS, Richardson MP, Koepp MJ. Identical, but not the same: intra-site and inter-site reproducibility of fractional anisotropy measures on two 3.0T scanners. Neuroimage. 2010;51(4):1384–94.
38. Frank LR. Characterization of anisotropy in high angular resolution diffusion-weighted MRI. Magn Reson Med. 2002;47(6):1083–99.
39. Wedeen VJ, Hagmann P, Tseng WY, Reese TG, Weisskoff RM. Mapping complex tissue architecture with diffusion spectrum magnetic resonance imaging. Magn Reson Med. 2005;54(6):1377–86.
40. Tuch DS. Q-ball imaging. Magn Reson Med. 2004;52(6):1358–72.

Publisher's Note Springer Nature remains neutral with regard to jurisdictional claims in published maps and institutional affiliations.